Enhanced late spring ozone in southern China by early onset of the South China Sea summer monsoon

Xiaorui Zhang[1], Xiao Lu[2], Fan Wang[1], Wen Zhou[3], Peng Wang[3], and Meng Gao[1]

[1]Department of Geography, Hong Kong Baptist University, Hong Kong, China.

[2]School of Atmospheric Sciences, Sun Yat-sen University, Guangzhou, China.

[3]Department of Atmospheric and Oceanic Sciences, Fudan University, Shanghai, China.

Corresponding author: Meng Gao (mmgao2@hkbu.edu.hk) and Xiao Lu (luxiao25@mail.sysu.edu.cn)

Key Points:

- Early onset of the South China Sea summer monsoon can create warmer and drier conditions with enhanced solar radiation in May.
- Enhanced chemical production dominates the worsening late spring ozone pollution in southern China during early onset events.
- Both sea surface temperature anomalies in the central equatorial Pacific and Philippine Sea contribute to higher ozone in southern China.

Abstract

The onset of the South China Sea summer monsoon (SCSSM) has profound impacts on meteorological conditions over East Asia. However, whether the interannual variability in monsoon onset date impacts ozone (O_3) pollution remains unclear. Here, we investigate the relationship between early onset of SCSSM and late spring O_3 in southern China. Our results show notable differences in surface O_3 concentrations before and after SCSSM onset during early onset events in southern China. The enhanced O_3 of 11.1 μg m^{-3} is supported by increased air temperature and solar radiation of 1.1 K and 30.9 W m^{-2} and reduced relative humidity of -5.7%. Both observation and model simulations confirm that O_3-favorable meteorological conditions modulated by early SCSSM onset can be found in May. It increases the boundary layer height and biogenic emissions of volatile organic compounds, enhancing O_3 by 10 μg m^{-3} over southern China. Chemical processes dominate such increases in O_3 with enhanced chemical production of 0.27 Tg $month^{-1}$. Descending motion in southern China vertically transports O_3 to surface by 0.10 Tg $month^{-1}$, whereas horizontal advection reduces O_3 concentration by 0.12 Tg $month^{-1}$. The meteorological responses to colder sea surface temperature (SST) in the central equatorial Pacific are pronounced, leading to higher O_3 concentrations over the Yangtze River Delta, while warmer SST in the Philippine Sea contributes O_3 over the Pearl River Delta and eastern China. This study highlights the importance of SCSSM onset with respect to O_3 in southern China, with promising applications in management of air pollution and agriculture.

Plain Language Summary

The onset of the South China Sea summer monsoon (SCSSM), a spectacular feature of the Asian summer monsoon, has significant impacts on meteorological conditions over East Asia. it remains unclear whether the interannual variability in monsoon onset date affects ozone (O_3) pollution. In this study, we demonstrated that the early onset of SCSSM can create warmer and drier conditions with enhanced solar radiation in May, which increases boundary layer height, boosts biogenic emissions of volatile organic compounds (VOC) and worsens O_3 pollution in southern China. By integrating reconstructed O_3 dataset and meteorological reanalysis together with model simulations, we found that increased O_3 concentrations of approximately 10 μg m^{-3} over southern China are dominated by enhanced chemical production. Both sea surface temperature anomalies in the central equatorial Pacific and Philippine Sea contribute to the O_3-favorable meteorological conditions modulated by early SCSSM onset. Our study emphasizes the importance of considering the SCSSM onset in understanding O_3 pollution in southern China, with promising applications in air pollution management and agriculture.

1 Introduction

Over the past two decades, China has suffered from severe air pollution as a result of rapid industrialization and urbanization (Chan & Yao, 2008; Gao et al., 2016; Huang et al., 2014). High levels of particulate matters ($PM_{2.5}$) and ozone (O_3) are greatly concerned by both the public and the Chinese government (Hong et al., 2019; Lelieveld et al., 2015; Zhang et al., 2019a). With the implementation of emission reduction measures since 2013, a reduction of 33% in $PM_{2.5}$ concentrations has been found in China (Gao et al., 2020b; Wang et al., 2020; Zhang et al., 2019a; Zhou et al., 2019), resulting in a decrease in $PM_{2.5}$-attributable premature deaths of 0.23 million from 2014 to 2020 (Wang et al., 2022). In contrast, increasing summer O_3 has emerged as a more prominent environmental challenge (Gao et al., 2020a; Li et al., 2019; Lu et al., 2018; Lu et al., 2020; Xiao et al., 2022). High levels of O_3 are found to harm human health, damage vegetation and reduce crop yields (Lippmann, 1989; Yue et al., 2017). O_3 exposure was responsible for approximately 64,370 premature respiratory mortalities in 69 Chinese cities in 2019 (Lu et al., 2020), and led to relative yield loss of 6% and 8% in wheat and rice across China in 2015 (Feng et al., 2019). Understanding the driving factors for O_3 pollution in China is thus crucial to policymakers.

Surface O_3 is primarily formed through photochemical reactions between volatile organic compounds (VOC) and nitrogen oxides (NO_x) in the presence of sunlight. In addition to emissions of precursors, regional weather conditions and large-scale circulation patterns also modulate O_3 concentrations (Liu et al., 2020; Lu et al., 2020; Wang et al., 2017; Yang et al., 2022; Yang et al., 2014; Yin & Ma, 2020). Generally, higher temperature and enhanced ultraviolet radiation accelerate photochemical reactions and promote emissions of biogenic precursors (Wang et al., 2017; Xiao et al., 2022), which were identified as dominant meteorological drivers for high summer O_3 in China (Wang et al., 2019; Yang et al., 2022; Zhang et al., 2022). The planetary boundary layer height (PBLH) also plays a significant role in vertical mixing (Dong et al., 2020), transport (Gao et al., 2019), and chemical reactions efficiency of O_3 (Zhang et al., 2023), showing a positive correlation with surface O_3 when PBLH is below 1 km (Han et al., 2020). Several studies recognized the significance of large-scale atmospheric circulation in the formation of O_3 pollution with a focus on summer. Higher summer O_3 anomalies (3-6 ppb) were found in central-eastern China due to enhanced transboundary transport during strong East Asian summer monsoon (EASM) years (Yang et al., 2014). Zhao and Wang (2017) argued that there was a negative correlation between O_3 over southern China and the intensity of the western Pacific subtropical high (WPSH), as a strong WPSH with large southwesterly anomalies would lead to more humid, cloudy and cooler conditions. Elevated summer O_3 levels in China were also linked to warm phases of El Niño-Southern Oscillation (ENSO) (Yang et al., 2022), positive phases of Eurasian teleconnection pattern, preceding May Arctic sea ice to the north of Eurasia (Yin et al., 2019), and variability in the joint movements of WPSH and East Asian deep trough (Yin & Ma, 2020). O_3 concentrations in late spring also exhibit relatively high levels in China (Lu et al., 2018; Zhao & Wang, 2017), and fast increasing trends were also identified (Li et al., 2021). However, climate factors that regulate late spring O_3 have not been well understood.

Weather and climate in southern China are largely affected by EASM, the commencement of which is characterized by abrupt shifts of low level zonal wind, precipitation, outgoing longwave radiation, and amount of clouds over the South China Sea (Ding & Chan, 2005; Wang et al., 2004). These changes during late spring indicate the onset of South China Sea summer monsoon (SCSSM hereafter for short) (Ding, 2007; Wang et al., 2009), which exhibits considerable inter-annual variability (Wang et al., 2004; Zhou & Chan, 2005). Previous studies have confirmed that the SCSSM onset plays a critical role in modulating meteorological conditions over East Asia. An early onset of SCSSM, often associated with La Niña, would lead to a northeastward shift of the WPSH (Huang et al., 2005; Zhang et al., 2019b; Zhou & Chan, 2007), a northward shift of the East Asian trough (Wang and Chen, 2018), and stronger convective activities around the Philippines (Kajikawa and Wang, 2012; Xiang and Wang, 2013). Such climate anomalies are generally accompanied by less East Asian monsoon rainfall over the lower reaches of the Yangtze River valley (He & Zhu, 2015) and increased frequency of tropical cyclones over the western Pacific (Kajikawa & Wang, 2012; Wang & Chen, 2018). These climate anomalies modulated by the onset of SCSSM might also affect O_3 concentrations in southern China, where O_3 is the most concerned pollutant with high values in spring (Gao et al., 2020a).

The responses of O_3 to monsoon have been well documented, yet whether the interannual variability in monsoon onset date impacts large-scale patterns of O_3 pollution remains unclear. Here we aim to understand how SCSSM onset affects late spring O_3 concentrations in southern China, and the associated implications for management of O_3 pollution. Using reconstructed O_3 dataset, meteorological reanalysis and numerical model simulations, we illustrate how meteorological conditions and variations of surface O_3 in southern China are modulated by the onset of SCSSM. Physical and chemical mechanisms for the modulation are also discussed.

2 Data and Methods

2.1 Reconstructed daily ground-level O_3 in China

Daily surface maximum 8 h average (MDA8) O_3 concentration in China from 2005 to 2021 was taken from Zhou et al. (2023) with a spatial resolution of 0.1°×0.1°. It was reconstructed using the extreme gradient boosting algorithm (XGBoost) with meteorological variables, anthropogenic emissions, land covers, etc, as inputs. Both cross validation and independent validation were conducted to confirm the accuracy of this dataset.

Considering the significant change in O_3 concentrations over study period due to emission reduction measures in China, we used the empirical mode decomposition (EMD) method to remove the influences of changing emissions in each grid (Gao et al., 2023). EMD can decompose O_3 variation into several physically meaningful components named Intrinsic Mode Functions (IMF) at different resolutions (Huang et al., 1998). We considered the last IMF with the lowest frequency as the signal associated with anthropogenic emission. We then removed this component to partly eliminate the effects of changing emissions. For example, the IMF 7 from EMD decomposition of O_3 concentrations over the North China Plain shows increasing trend during 2013-2017 and a reversal after it, which agrees with the trend of anthropogenic driver concluded by Li et al. (2020). It is important to note that this detrending approach may not completely eliminate the impact of human emissions, but it helps to focus our investigation on the influence of the SCSSM onset on O_3 concentrations.

2.2 Meteorological reanalysis data and definition of SCSSM onset

Daily meteorological variables with a horizontal resolution of 2.5°×2.5° over 1979-2021 were obtained from the National Centers for Environmental Prediction–Department of Energy (NCEP-DOE) reanalysis dataset (Kanamitsu et al., 2002). We included sea level pressure, zonal and meridional winds, near-surface humidity, temperature, and downward solar radiation at the surface in this study, which have been shown in previous studies to play the most important roles in photochemical pollution in China (Zhang et al., 2022). Monthly sea surface temperature (SST) with a spatial resolution of 0.25°×0.25° was taken from the European Centre for Medium-Range Weather Forecasts (ECMWF) ERA-5 reanalysis dataset (Hersbach et al., 2020).

The onset of SCSSM was defined as the day after April 1 that satisfies steady easterly to westerly shift of zonal winds averaged over South China Sea (5°-15°N, 110°-120°E) at 850 hPa (Wang et al., 2004), using the NCEP-DOE reanalysis dataset. Such a shift means that the 850 hPa zonal winds in this region become positive and maintain at least two pentads (10 days). The SCSSM onset dates, shown in Table 1, exhibit a distinguished interannual variation. Years with anomalous SCSSM onset date earlier (later) than one standard deviation were selected as early (late) SCSSM onset events in this study (Jiang et al., 2018).

Table 1. Dates of South China Sea summer monsoon.

Year	Onset date (anomaly)	Year	Onset date (anomaly)	Year	Onset date (anomaly)
1979	13-May (-7)	1994#	2-May (-18)	2009#	16-Apr (-34)
1980	13-May (-7)	1995	12-May (-8)	2010	22-May (-2)
1981	1-Jun (12)	1996#	7-May (-13)	2011	23-May (-3)
1982	1-Jun (12)	1997	18-May (-2)	2012	20-May (0)
1983*	17-Jun (28)	1998	20-May (0)	2013*	8-Jun (19)
1984*	7-Jun (18)	1999	23-May (3)	2014*	5-Jun (16)
1985	27-May (7)	2000#	7-May (-13)	2015*	16-Jun (27)
1986	11-May (-9)	2001	8-May (-12)	2016	20-May (0)
1987*	7-Jun (18)	2002	15-May (-5)	2017	16-May (-4)
1988	20-May (0)	2003	15-May (-5)	2018	1-Jun (12)

1989	17-May (-3)	2004	8-May (-12)	2019#	1-May (-19)
1990	17-May (-3)	2005	26-May (6)	2020	21-May (1)
1991*	8-Jun (19)	2006	12-May (-8)	2021	20-May (0)
1992*	12-Jun (23)	2007	20-May (0)	Mean	20-May
1993*	5-Jun (16)	2008#	1-May (-19)	SD	12.5 days

and * denote years that selected as the early and late onset events. SD represents the standard deviation of anomalous SCSSM onset dates.

2.3 Numerical model experiments

The Community Earth System Model (CESM) version 2.1.3 was employed to explore the responses of O_3 pollution over China to the onset of SCSSM, with a horizontal resolution of 0.94° × 1.25° and 70 vertical layers (Gent et al., 2011). The atmospheric components were provided by Community Atmosphere Model version 6 (CAM6), while chemical and land processes were simulated by the Whole Atmosphere Community Climate Model version 6 (WACCM6), and the Community Land Model version 5 (CLM5), respectively. Anthropogenic emissions were provided by the Community Emissions Data System (Hoesly et al., 2018). Biogenic emissions were calculated online by the Model of Emissions of Gases and Aerosols from Nature (MEGAN) version 2.1. This study conducted a control case with SST data from monthly varying climatology ($CESM_{ctrl}$), and a sensitivity simulation by imposing the SST anomaly patterns associated with early SCSSM onset events ($CESM_{early}$). Two additional sensitivity simulations were conducted by imposing a warmer SST of 0.6 K over the Philippine Sea (0°N-20°N, 120°E-160°E, $CESM_{PhiSea}$) and colder SST of -1.0 K over central equatorial Pacific (5°S-5°N, 160°E-150°W, $CESM_{CenPacif}$). All simulations were conducted from January to June 2010. The year 2010 was selected because it did not exhibit an early or late SCSSM onset (Table 1), and had small SST anomalies (Gao et al., 2023; Hu et al., 2022). We evaluated the $CESM_{ctrl}$ based on mean fractional bias (MFB) and the mean fractional error (MFE) (Boylan and Russell, 2006). The CESM model can reproduce the general variations of important meteorological factors and O_3 in southern China, with MFB within ±0.18 and MFE lower than 0.30. Given these uncertainties and biases in CESM simulation, simulated results were mainly used to investigate the direction of the response rather than the magnitude of the influence.

3 Results and discussion

3.1 Impacts of early SCSSM onset on O_3 in southern China

The onset of SCSSM generally occurs in late spring, preceded by persistent springtime rainfall over southeastern China (Wan & Wu, 2007), and followed by northward movement of the rain belt (Ding & Chan, 2005). To estimate the variation in O_3 concentrations following the onset of SCSSM, the average O_3 concentrations for 15 days after the onset were subtracted from those for 15 days preceding the onset date, as illustrated in Figure 1. Enhanced O_3 concentration of 20 μg m^{-3} is commonly observed over eastern China within three pentads (15-day average) after onset dates during 2005-2021 (Figure 1a). During early onset events, O_3 concentrations in southern China experience overall enhancements after onsets, with the largest increase of more than 26 μg m^{-3} in the Yangtze River Delta (YRD) and Pearl River Delta (PRD) (Figure 1b). The frequency of high O_3 days (MDA8 O_3 concentrations exceeded 100 μg m^{-3}) is also increased by 4 days within three pentads in southern China after early onset dates. In contrast, no significant differences in O_3 concentrations for late onset events are found (Figure 1c).

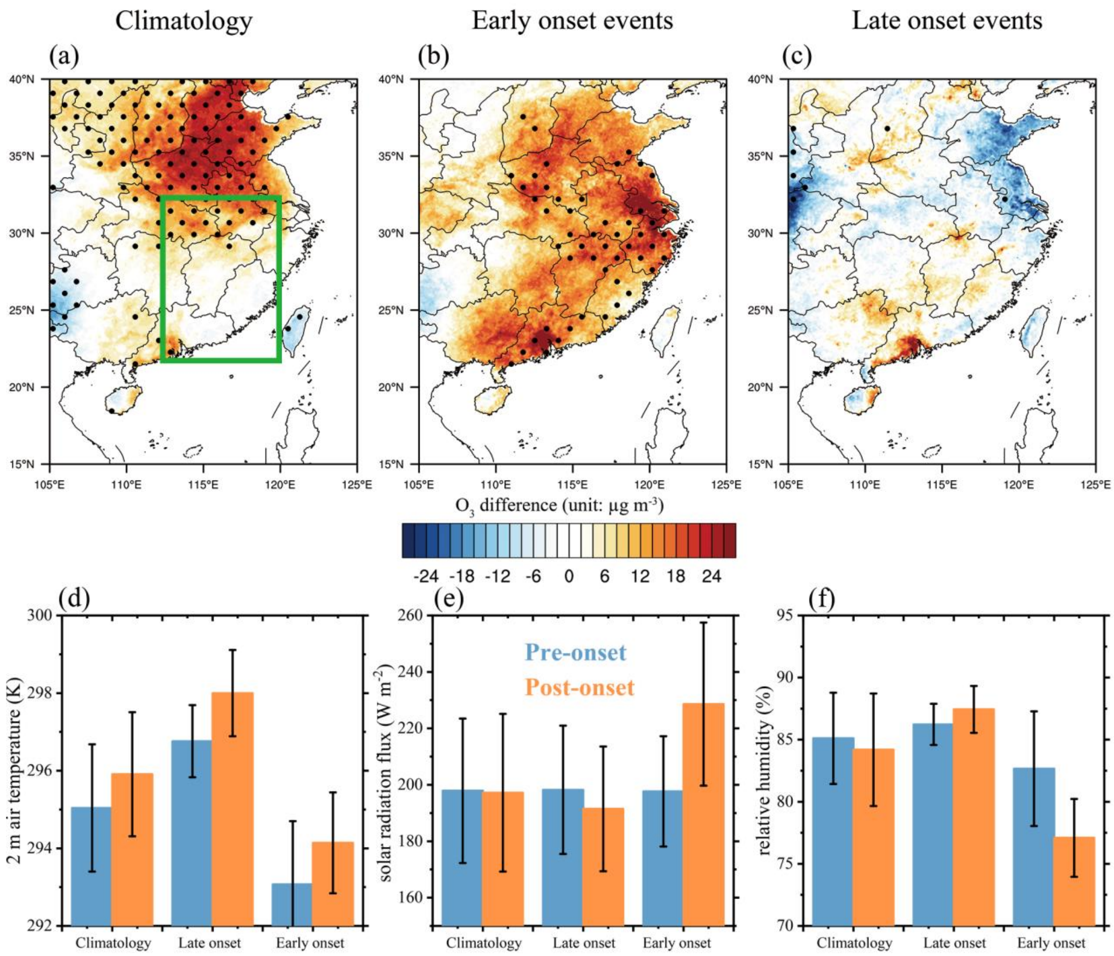

Figure 1. Differences in surface O_3 and associated weather conditions over southern China between the pre-onset and post-onset of SCSSM for different phases of SCSSM onset. Three-pentad averaged (15-days average) differences in surface O_3 concentrations (μg m^{-3}) between after (during onset to onset date + 15 days) and before (during onset to onset date - 15 days) the SCSSM onset for (a) climatological mean, (b) early onset events and (c) late onset events during 2005-2021, respectively (Green box marks southern China). Dotted areas represent statistical

significance with 95% confidence according to Student's t test. (d) Comparisons of three pentad averaged 2 m air temperature (K) over southern China (the green box shown in Figure 1a) during pre-onset and post-onset of SCSSM for climatological mean, early onset events and late onset events during 1979-2021, respectively. (e) Same as (d) but for surface downward solar radiation flux (W m^{-2}). (f) Same as (d) but for near-surface relative humidity (%).

We examined the corresponding differences in meteorological parameters relevant to O_3 formation between post- and pre-onset of SCSSM. Following the onset of SCSSM during climatology, the negative anomalous sea level pressure in South China Sea induces not only easterly to westerly shift over South China Sea, but also northeasterly winds over southeastern China, weakening moisture transport. Downward solar radiation and temperature increase together with reduced humidity over the North China Plain after onset, favoring O_3 production. For early onset events, the stronger cyclonic circulation located in the Philippine Sea results in more O_3-favorable conditions than those of climatology mean. Specifically, obvious differences are observed in early onset event that the air temperature and solar radiation are increased by 1.1 K and 30.9 W m^{-2}, respectively, accompanied by a considerable decrease of 5.7% in relative humidity (Figure 1). Such shifts in meteorological parameters in early onset events contribute to an increase in surface O_3 concentrations of 11.1 μg m^{-3} over southern China, which are not consistent in late onset events. This reflects the different processes for the early and late onsets of SCSSM. Early SCSSM onsets are generally associated with northwestward-moving tropical convection, whereas late SCSSM onset is primarily affected by the northward migration of the intertropical convergence zone (Kajikawa & Wang, 2012).

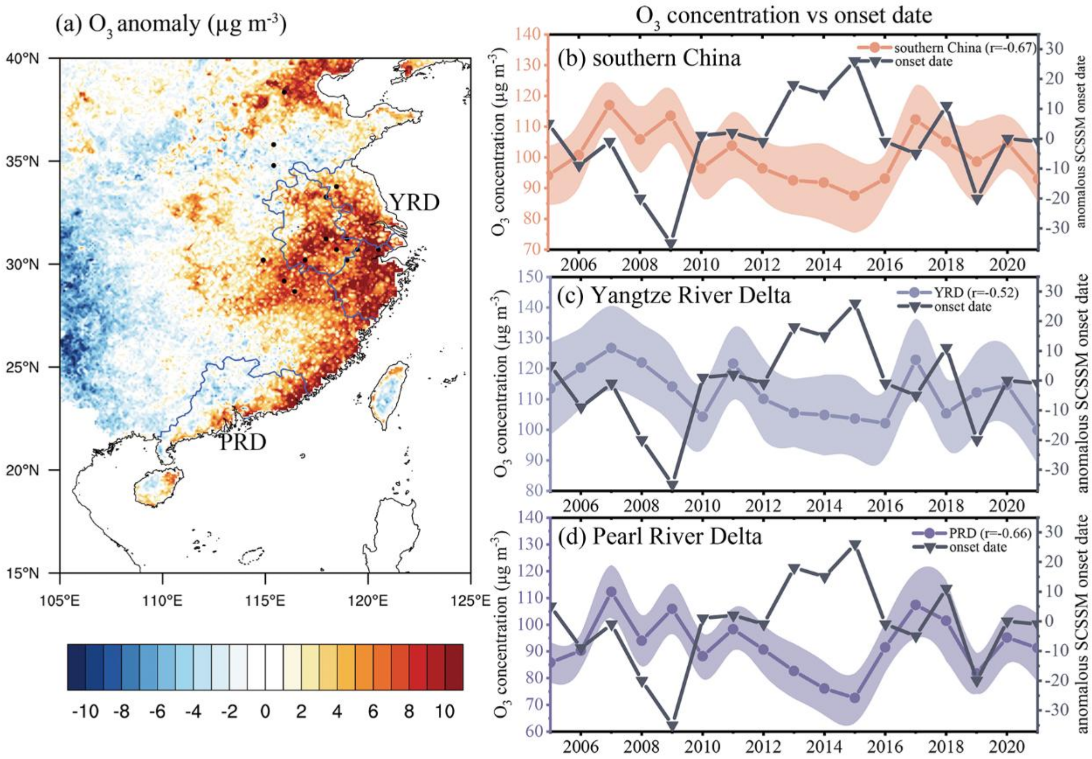

Figure 2. Early onset events modulated surface O_3 in May. (a) Composite difference of O_3 (μg m^{-3}) in May between early SCSSM onset events and climatological mean. Dotted areas represent statistical significance with 95% confidence according to Student's t test. Time series of the anomalous SCSSM onset date and O_3 (μg m^{-3}) in May over (b) southern China, (c) Yangtze River Delta (YRD), and (d) Pearl River Delta (PRD), respectively.

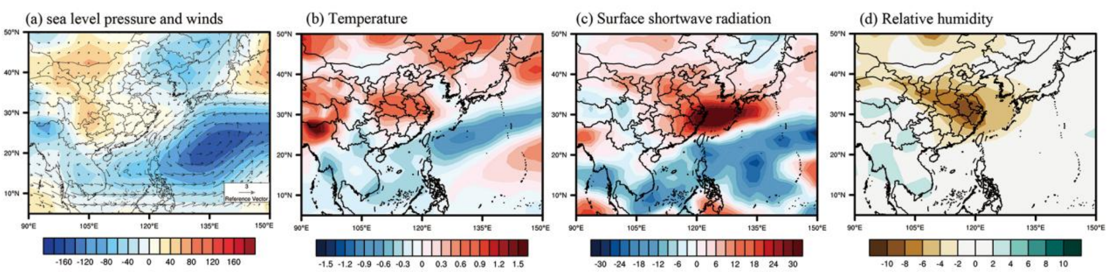

Figure 3. The impacts of early SCSSM onset events on meteorological conditions in May. Composite difference of (a) sea level pressure (Pa, contour) and wind fields

(m s^{-1}, vector) at 850 hPa, (b) 2 m air temperature (K), (c) surface downward solar radiation flux (W m^{-2}) and (d) near-surface relative humidity (%) in May between early SCSSM onset events and climatological mean over 1979-2021.

As mentioned above, early SCSSM onset accompanied with O_3-favorable meteorological conditions significantly increases surface O_3 over southern China. We further investigate the impacts of early SCSSM onset on O_3 in May when SCSSM onset dates mainly happened (Table 1). In southern China, there has been an increase of approximately 5 high O_3 days in May due to the early SCSSM onset. Based on the detrended O_3 data by EMD method, the composite difference in May O_3 between early SCSSM onset events and climatological mean witnesses a remarkable rise of higher than 5 μg m^{-3} over southern China (Figure 2a). Statistically significant correlation between surface O_3 in May and the anomalous SCSSM onset dates during 2005-2021 can be found in YRD, PRD and southern China with correlation coefficients of -0.52, -0.66 and -0.67, respectively (Figure 2). However, it is worth noting that despite the occurrence of an early onset event in 2019, the O_3 concentrations were relatively low during this period. This deviation can be attributed to the fact that the early onset event in 2019 was triggered by a cold front, unlike most early onset events that are typically triggered by tropical convection (Hu et al., 2020). On May 1st, 2019 (the onset date of SCSSM), a strong cold front extended from Japan to the South China Sea (Hu et al., 2020). Southern China was affected by strong northerly winds after the cold front. The intrusion of cold air from the north significantly inhibited the photochemical reactions responsible for O_3 formation, ultimately leading to the observed lower surface O_3 concentrations. Without considering the early onset event in 2019, we found that early onset events during the period from 2005 to 2021 tend to increase the O_3 concentration in May over YRD, PRD and southern China by 6.1, 8.1 and 9.3 μg m^{-3} (Figure 2). The high values of O_3 anomaly are overlapped with the composite differences in meteorological conditions (Figure 3). Warmer and drier conditions in May are found over southern China during early onset events with surface temperature increased by 0.8 K and relative humidity reduced by 9% compared to the climatological mean (Figure 3b and d). Stronger shortwave radiation fluxes of higher than 30 W m^{-2} appear in the YRD (Figure 3c).

3.2 Mechanism for the impacts of early SCSSM onset on late spring O_3 in southern China

We employed CESM experiments to investigate the influences of early SCSSM onset, which would be helpful to elucidate the underlying mechanisms responsible for the observed changes in surface O_3 associated with early SCSSM onset. SST during February-March-April (FMA) play dominant roles in the variation of the SCSSM onset (Hu et al., 2022; Kajikawa & Wang, 2012). A sensitivity simulation ($CESM_{early}$) was conducted by imposing the SST anomaly patterns associated with early SCSSM onset events (Figure 4). The differences between $CESM_{early}$ and $CESM_{ctrl}$ were regarded as the influence of early SCSSM onset.

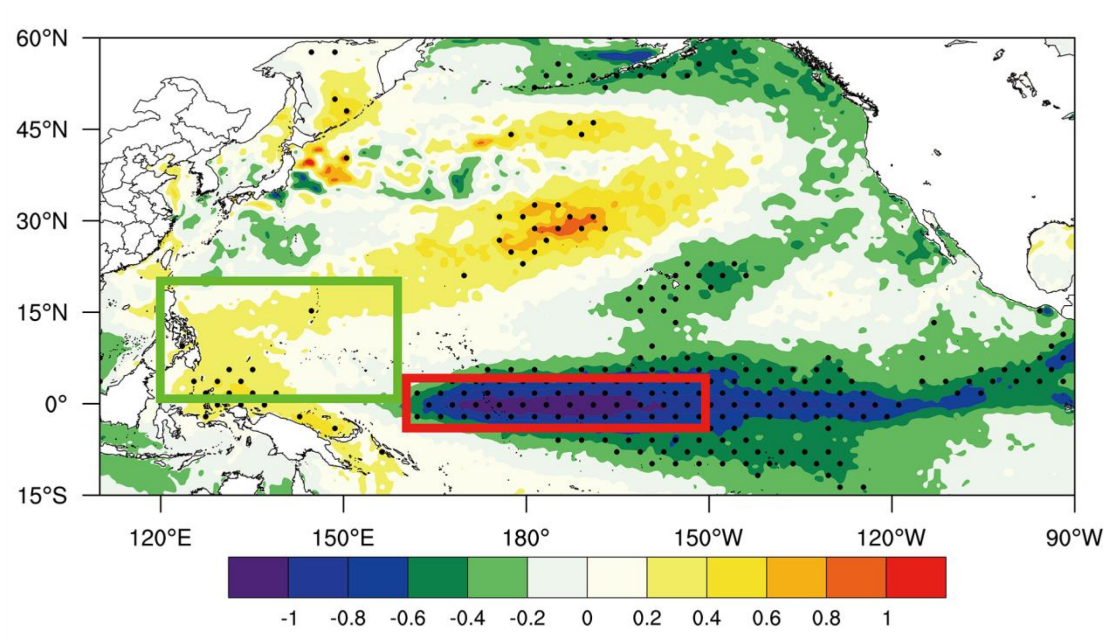

Figure 4. Composite difference of February-March-April (FMA) averaged sea surface temperature (K) between early SCSSM onset events and climatological mean over 1979-2021 (The green and red box represent the region with SST anomaly imposed in $CESM_{PhiSea}$ and $CESM_{CenPacif}$, respectively).

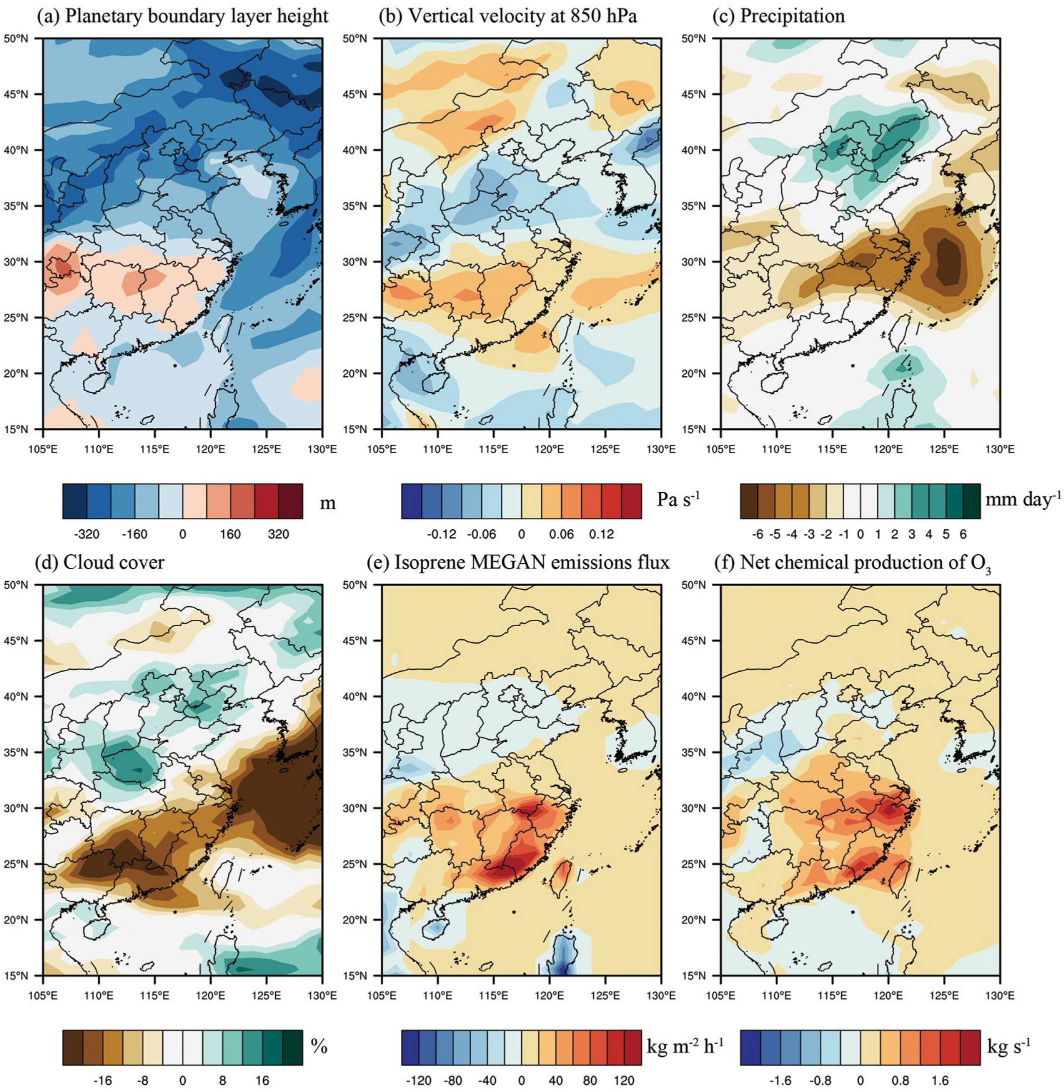

Figure 5. CESM simulated responses to early onset event. CESM simulated responses of (a) planetary boundary layer height (PBLH, m), (b) vertical pressure velocity at 850 hPa (Pa s^{-1}), (c) precipitation (mm day^{-1}), (d) cloud cover (%), (e) isoprene emissions flux (kg m^{-2} h^{-1}) from MEGAN and (f) net chemical production of O_3 (kg s^{-1}) in May to early onset event.

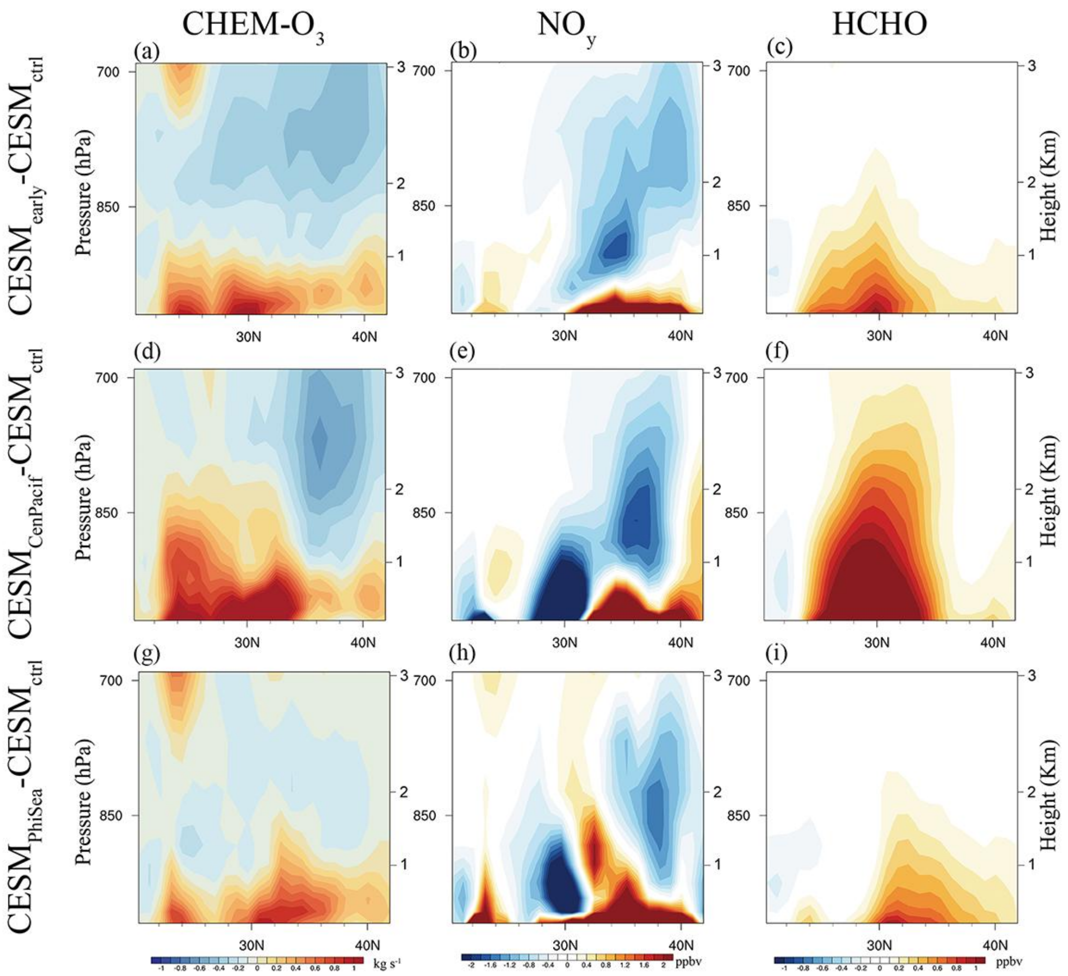

Figure 6. CESM simulated responses of profiles of O_3 chemical conditions. CESM simulated responses profile of (a, d, g) net chemical production of O_3 (kg s^{-1}), (b, e, h) total reactive nitrogen oxides (NO_y =NO_x+HONO+HNO_2+HNO_3+HNO_4), and (c, f, i) formaldehyde (HCHO) in May to early onset event (top panels), colder SST over central equatorial Pacific (middle panels), warmer SST over Philippine Sea (bottom panels).

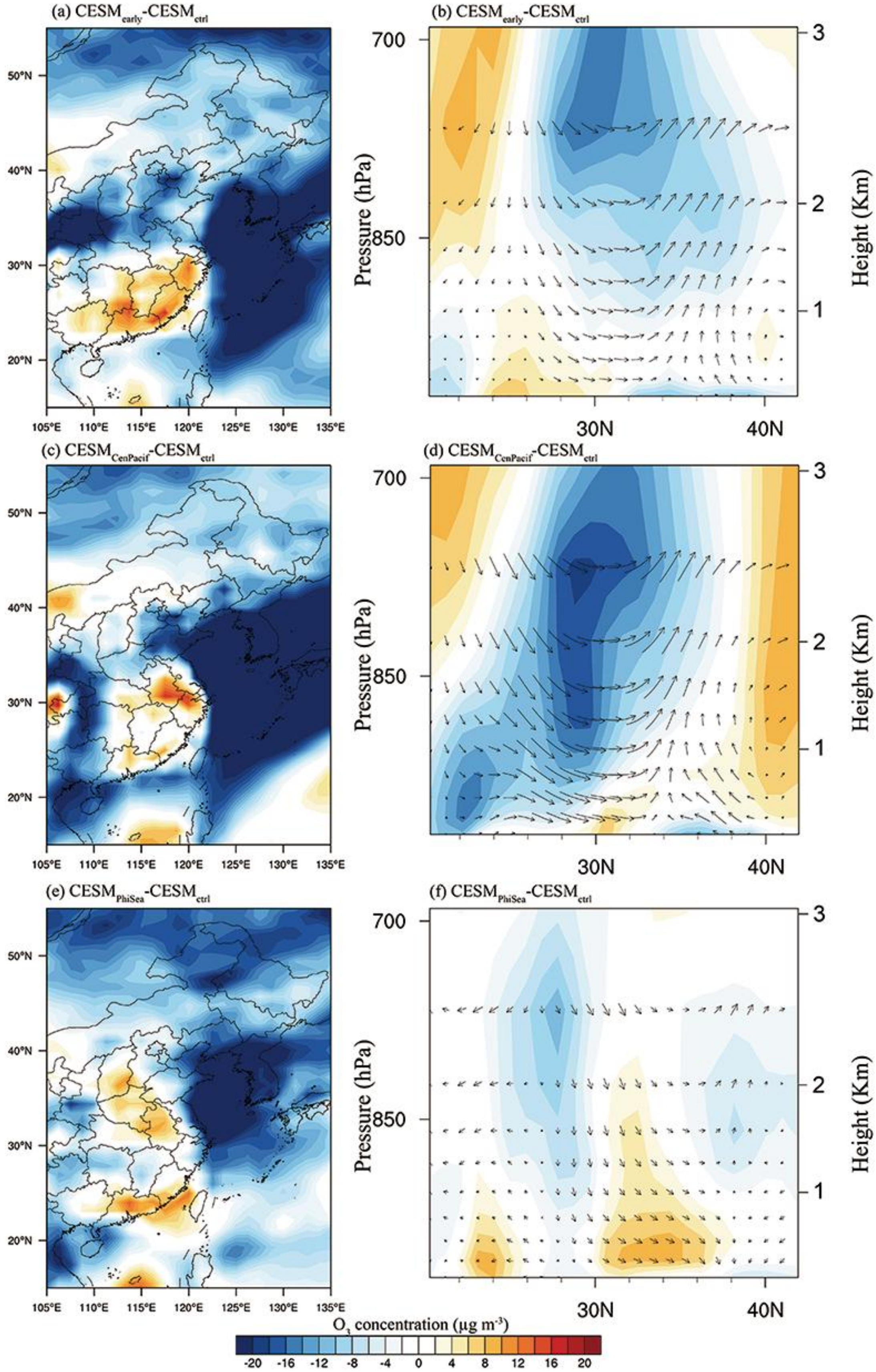

325

326 **Figure 7. CESM simulated responses of O_3 concentrations.** CESM simulated

responses of horizontal distribution of near-surface O_3 concentration and pressure-longitude cross sections averaged over 112.5-120°E of O_3 concentration (μg m^{-3}, contour) and winds (m s^{-1}, vector) in May to (a, b) early onset event, (c, d) colder SST over central equatorial Pacific, (e, f) warmer SST over Philippine Sea.

The steady shift in zonal wind at 850 hPa over the South China Sea from $CESM_{early}$ occurs on 2 May, which is advanced by 20 days compared to $CESM_{ctrl}$. The simulated responses are consistent with the results obtained from reanalysis data, affirming that the impacts of early onset events on meteorological conditions and O_3 enhancements can be successfully reproduced by our simulations. The early onset of SCSSM induces a cyclonic anomaly over the South China Sea, resulting in reduced water vapor entering southern China. It decreases cloudiness by 20% (Figure 5d), allowing an additional solar radiation of 50 W m^{-2} to reach the surface. Precipitation is also suppressed by -5 mm per day over the YRD (Figure 5c), accompanied by a 4 K increase in surface temperature. In addition, biogenic VOC emissions from a broad area of forest in southern China are also boosted by higher temperature (Figure 6c), exhibiting enhanced isoprene emission fluxes of 60 kg m^{-2} h^{-1} calculated by the MEGAN (Figure 5e). We use the index based on the ratio of the concentration of HCHO and NO_y (Sillman, 1995), and find that VOC-limited regime dominates southern China at surface. With more VOCs available for reactions with NO_x, the photochemical reactions are substantially accelerated by 1 kg s^{-1} (Figure 5f). Consequently, the responses of surface O_3 concentration to early onset of SCSSM are in line with the meteorological and VOC emissions anomalies, presenting the largest increases exceeding 12 μg m^{-3} over southern China (Figure 7a).

Higher solar radiation and temperature in southern China during early onset event promote the development of boundary layer. Accordingly, PBLH increases by 80 m in southern China but decreases by 100 m in northern China (Figure 5a). These changes in PBLH can affect vertical mixing and transport of O_3 as well as its precursors. O_3 precursors such as total reactive nitrogen oxides (NO_y) and formaldehyde (HCHO) in northern China are trapped near the surface due to lower PBLH, but are more effectively dispersed with higher PBLH in southern China (Figure 6). The O_3 formation sensitivity in the lower troposphere is NO_x-limited regime over the south of 29 °N, and VOC-limited regime over the north of 29°N. Positive anomalies of 0.4 ppb for NO_y and 0.8 ppb for HCHO are observed below 1 km near 26 °N and 30 °N, respectively. These anomalies significantly strengthen net chemical production of O_3 within the PBLH (Figure 6a), contributing to O_3 anomalies of 4 μg m^{-3} at a height of 1 km above the surface over southern China (Figure 7b).

Table 2 summarizes the contributions from physical and chemical processes to surface O_3 in southern China. The descending motion anomalies of 0.06 Pa s^{-1} over southern China vertically transport O_3 to surface by 0.10 Tg $month^{-1}$ (Figure 5b). The

O_3 export fluxes of 0.14 Tg month^{-1} to northern China indicate that the horizontal advection plays a negative role in O_3 concentration in southern China (Table 2). The increases in O_3 over southern China are primarily driven by chemical processes with the enhanced net chemical production of 0.27 Tg month^{-1}.

Table 2. Mean O_3 vertical and horizontal fluxes (unit: Tg month^{-1}) at different edges of southern China (the green box shown in Figure 1a) and net O_3 chemical production (unit: Tg month^{-1}) at surface. Positive (negative) values indicate incoming (outgoing) O_3 flux.

	$CESM_{early}$-$CESM_{ctrl}$	$CESM_{CenPacif}$-$CESM_{ctrl}$	$CESM_{PhiSea}$-$CESM_{ctrl}$
		Horizontal flux	
East	0.059	-0.050	0.124
West	-0.037	0.038	-0.085
North	-0.143	-0.355	-0.073
South	0.005	0.043	-0.009
		Vertical flux	
Top	0.101	0.352	0.029
		Net chemical production	
	0.271	0.409	0.167

3.3 Influences of SST anomalies associated with early onset events

Previous studies demonstrated the crucial role of SST anomalies during February-March-April (FMA) in the equatorial Pacific and the Philippine Sea in modulating the onset date of SCSSM (Hu et al., 2022; Kajikawa and Wang, 2012; Xiang and Wang, 2013). In this study, we further investigated the impacts of SST anomalies in these regions on O_3. As shown in Figure 4, the spatial pattern of FMA-averaged SST anomalies for early onset events resembles the La Niña pattern. Most prominent SST signals are observed in the central equatorial Pacific within 5°S and 5°N, where eminently negative SST anomalies are lower than 1 K within 160°E and 150°W, labeled as the Niño 4 region (Figure 4). The simulated responses of meteorological conditions to such colder SST are similar to those during early onset event, but with greater magnitudes. The contribution from net O_3 chemical production is 0.41 Tg month^{-1}, exceeding that from $CESM_{early}$ (Table 2). This enhancement is supported by higher solar radiation and surface temperature of 20 W m^{-2} and 3 K than $CESM_{early}$. Moreover, the responses of PBLH and biogenic VOC emissions from $CESM_{CenPacif}$ are also more pronounced than those from $CESM_{early}$ in southern China. As a consequence, the vertical distribution of HCHO and NO_y spans a broader range in the atmosphere (Figure 6e, f). The net chemical production anomalies are greater than 1 kg s^{-1} below 1 km over southern China, and reach up to 0.2 kg s^{-1} at 2 km above the surface (Figure 6d). The descending motion and northerly anomalies are much stronger, contributing to surface O_3 by 0.35 and -0.36 Tg month^{-1} respectively (Table 2). Although chemical production is enhanced over southern China, physical processes transport O_3 towards north boundary. Accordingly, the positive response of surface O_3 to colder SST in the central equatorial Pacific is mainly concentrated in YRD.

Statistically significant positive SST anomalies of up to 0.6 K appear in the Philippine Sea (Figure 4), which has been illustrated to advance SCSSM onset also (Kajikawa & Wang, 2012; Xiang & Wang, 2013). Although ENSO is typically the most important factor regulating SCSSM onset, their relationship has become weak in recent decades, as reported by Hu et al. (2022). Kajikawa and Wang (2012) identified the warming of the Philippine as the root cause of the interdecadal advance of SCSSM. The SCSSM onset date is obviously advanced by 15 days due to warmer SST in the Philippine Sea. O_3-favorable meteorological conditions over southern China have been found in $CESM_{PhiSea}$ but much weaker than those in $CESM_{early}$ and $CESM_{CenPacif}$, leading to net chemical production of 0.17 Tg month^{-1} (Table 2). The temperature and solar radiation are also enhanced in north of 30 °N by 2K and 20 W m^{-2}, slightly promote an increase of 60m in PBLH. Positive HCHO anomalies are accordingly found in north of 30 °N (Figure 6i), which is VOC-limited regime. Thus, the surface chemical production anomalies mainly in PRD and eastern China, with increased O_3 concentrations of 12 and 8 μg m^{-3}, respectively (Figure 7e).

It is noteworthy that the simulated responses of O_3 in $CESM_{CenPacif}$ are larger than those in $CESM_{early}$, and both are consistent with the observed O_3 anomalies during early onset events (Figure 2a). However, the responses in $CESM_{PhiSea}$ align more closely with the changes in O_3 during all onset events (Figure 1a), displaying positive anomalies in PRD and eastern China. The SST in the Philippine Sea can modulate the convective activities to further influence SCSSM onset date, showing a warming trend of 0.02 K year^{-1} from 1979 to 2021. Therefore, the most of SST anomalies were positive during the study period (2005-2021), leading to higher O_3 in PRD and eastern China. These results suggest that SST anomalies in the central equatorial Pacific exhibit significant impacts during early onset events, whereas O_3 variations during most of the SCSSM onsets are linked to SST anomalies in the Philippine Sea in recent decades.

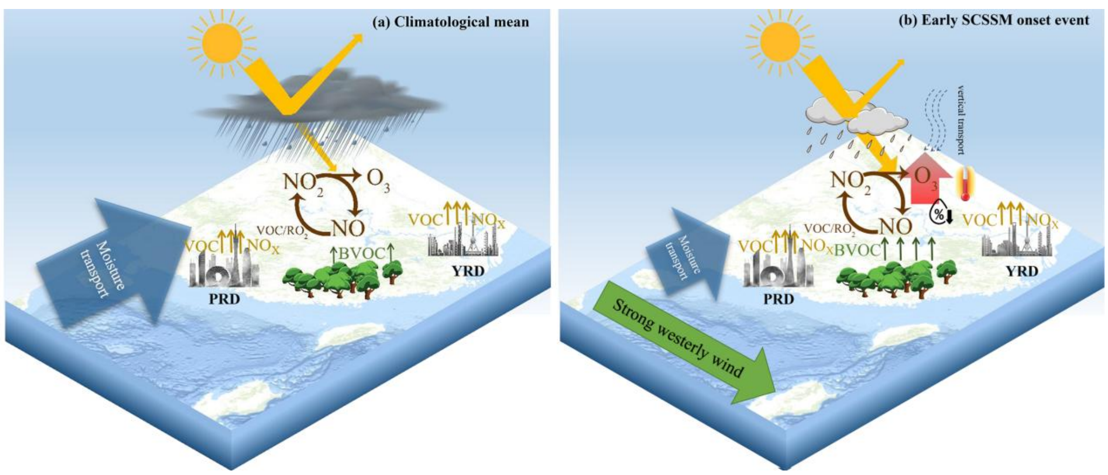

Figure 8. Conceptual scheme of modulation of O_3 in Southern China by early SMSSM onset. Meteorological conditions and chemical processes of O_3 during (a) climatological mean and (b) early SCSSM onset event.

4 Conclusions

The onset of SCSSM is the most important sub-seasonal phenomenon of the EASM system. Anomalies in circulation patterns and meteorological conditions modulated by the variability of SCSSM onset also affect O_3 pollution in China, which have been less explored. In this study, we illustrate how early SCSSM onset affects late spring O_3 over southern China based on a reconstructed surface O_3 dataset and meteorological reanalysis, and further investigate the mechanisms through CESM simulations. It should be noted that the O_3 dataset was reconstructed using XGBoost, and detrended by EMD method.

Notable differences in surface O_3 concentrations and associated meteorological conditions before and after SCSSM onset during early onset events are observed over southern China. Following the early onset of SCSSM, increased air temperature and solar radiation by 1.1 K and 30.9 W m^{-2}, together with the decrease of 5.7% in relative humidity contribute to an increase of 11.1 μg m^{-3} in surface O_3 concentrations over southern China. The O_3-favorable meteorological conditions accompanied by early SCSSM onset are also found in May, creating a warmer (0.8 K) and drier (-9%) condition associated with stronger solar radiation (30 W m^{-2}) over southern China compared to the climatological mean. Thus, O_3 concentration in May is negatively related to the onset date of SCSSM, with an increase of 9.3 μg m^{-3} over southern China during early onset events.

CESM experiments show that early SCSSM onset increases surface O_3 concentration in May by over 12 μg m^{-3} over southern China, and the influences are extended to middle troposphere. Chemical processes play dominant roles in the increases in O_3 with enhanced net chemical production of 0.27 Tg $month^{-1}$, which is supported by warmer and drier conditions with enhanced solar radiation and less precipitation. Higher temperature associated with early onset events also increases PBLH and boosts biogenic emissions of VOCs from a broad area of forest in southern China. Although descending motion vertically transports O_3 from troposphere to surface layer by 0.10 Tg $month^{-1}$, physical processes exhibit negative impacts on O_3 concentrations mainly due to horizontal advection.

SST during FMA featuring early onset of SCSSM event are colder of -1 K in the central equatorial Pacific and warmer of 0.6 K in the Philippine Sea than climatological mean. The colder SST in the central equatorial Pacific causes more O_3-favorable meteorological conditions and enhances O_3 chemical production by 0.41 Tg $month^{-1}$. However, physical processes transport O_3 towards the north boundary, resulting in outgoing fluxes of 0.36 Tg month^{-1}. Consequently, the SST anomalies in the central equatorial Pacific mainly increase surface O_3 concentrations in YRD, while higher O_3 concentrations in PRD are attributed by SST anomalies in the Philippine Sea. Colder SST in the central equatorial Pacific has significant impacts on O_3 over southern China during early onset events, whereas variations in O_3 during most of the SCSSM onsets are related to SST anomalies in the Philippine Sea in recent decades.

Our results highlight the significant role of SCSSM onset in modulating surface O_3 pollution in late spring in southern China, as summarized in Figure 8. Considering the adverse impacts of O_3 on food production and human health, our conclusion suggests promising applications in management of O_3 pollution and agriculture.

Acknowledgments

This work is supported by Research Grants Council of the Hong Kong Special Administrative Region, China (project no. HKBU22201820 and HKBU12202021), National Natural Science Foundation of China (No. 42005084) and National Key Research and Development Programs of China (No. 2022YFC3700103).

Open Research

The reconstructed daily ground-level O_3 data are available at Zenodo via https://zenodo.org/record/7766129#.ZCGXAHZBw7F. Meteorological data are available from https://psl.noaa.gov/data/gridded/data.ncep.reanalysis2.html and monthly SST can be obtained from https://cds.climate.copernicus.eu/cdsapp#!/dataset/reanalysis-era5-single-levels-monthly-means.

References:

Boylan, J. W., & Russell, A. G. (2006). PM and light extinction model performance metrics, goals, and criteria for three-dimensional air quality models. *Atmospheric environment*, 40(26), 4946-4959.

Chan, C. K., & Yao, X. (2008). Air pollution in mega cities in China. *Atmospheric environment, 42*(1), 1-42.

Ding, Y. (2007). The variability of the Asian summer monsoon. *Journal of the*

Meteorological Society of Japan. Ser. II, 85, 21-54.

Ding, Y., & Chan, J. C. (2005). The East Asian summer monsoon: an overview. *Meteorology and Atmospheric Physics, 89*(1), 117-142.

Dong, Y., Li, J., Guo, J., Jiang, Z., Chu, Y., Chang, L., et al. (2020). The impact of synoptic patterns on summertime ozone pollution in the North China Plain. Science of the Total Environment, 735, 139559.

Feng, Z., De Marco, A., Anav, A., Gualtieri, M., Sicard, P., Tian, H., et al. (2019). Economic losses due to ozone impacts on human health, forest productivity and crop yield across China. Environment International, 131, 104966.

Gao, D., Xie, M., Chen, X., Wang, T., Zhan, C., Ren, J., & Liu, Q. (2019). Modeling the effects of climate change on surface ozone during summer in the Yangtze River Delta region, China. International Journal of Environmental Research and Public Health, 16(9), 1528.

Gao, M., Carmichael, G., Wang, Y., Saide, P., Yu, M., Xin, J., et al. (2016). Modeling study of the 2010 regional haze event in the North China Plain. *Atmospheric Chemistry and Physics, 16*(3), 1673-1691.

Gao, M., Gao, J., Zhu, B., Kumar, R., Lu, X., Song, S., et al. (2020a). Ozone pollution over China and India: seasonality and sources. *Atmospheric Chemistry and Physics, 20*(7), 4399-4414.

Gao, M., Liu, Z., Zheng, B., Ji, D., Sherman, P., Song, S., et al. (2020b). China's emission control strategies have suppressed unfavorable influences of climate on wintertime PM 2.5 concentrations in Beijing since 2002. *Atmospheric Chemistry and*

Physics, 20(3), 1497-1505.

Gao, M., Wang, F., Ding, Y., Wu, Z., Xu, Y., Lu, X., et al. (2023). Large-scale climate patterns offer preseasonal hints on the co-occurrence of heat wave and O3 pollution in China. *Proceedings of the national academy of sciences*, 120(26), e2218274120.

Gent, P. R., Danabasoglu, G., Donner, L. J., Holland, M. M., Hunke, E. C., Jayne, S. R., et al. (2011). The community climate system model version 4. *Journal of Climate, 24*(19), 4973-4991.

Han, H., Liu, J., Shu, L., Wang, T., & Yuan, H. (2020). Local and synoptic meteorological influences on daily variability in summertime surface ozone in eastern China. Atmospheric Chemistry and Physics, 20(1), 203-222.

He, J., & Zhu, Z. (2015). The relation of South China Sea monsoon onset with the subsequent rainfall over the subtropical East Asia. *International Journal of Climatology, 35*(15), 4547-4556.

Hersbach, H., Bell, B., Berrisford, P., Hirahara, S., Horányi, A., Muñoz-Sabater, J., et al. (2020). The ERA5 global reanalysis. *Quarterly Journal of the Royal Meteorological Society, 146*(730), 1999-2049.

Hoesly, R. M., Smith, S. J., Feng, L., Klimont, Z., Janssens-Maenhout, G., Pitkanen, T., et al. (2018). Historical (1750–2014) anthropogenic emissions of reactive gases and aerosols from the Community Emissions Data System (CEDS). *Geoscientific Model Development*, 11(1), 369-408.

Hong, C., Zhang, Q., Zhang, Y., Davis, S. J., Tong, D., Zheng, Y., et al. (2019). Impacts of climate change on future air quality and human health in China.

Proceedings of the National Academy of Sciences, 116(35), 17193-17200.

Hu, P., Chen, W., Chen, S., Liu, Y., & Huang, R. (2020). Extremely early summer monsoon onset in the South China Sea in 2019 following an El Niño event. *Monthly Weather Review, 148*(5), 1877-1890.

Hu, P., Chen, W., Chen, S., Wang, L., & Liu, Y. (2022). The weakening relationship between ENSO and the South China Sea summer monsoon onset in recent decades. *Advances in Atmospheric Sciences, 39*(3), 443-455.

Huang, N. E., Shen, Z., Long, S. R., Wu, M. C., Shih, H. H., Zheng, Q., et al. (1998). The empirical mode decomposition and the Hilbert spectrum for nonlinear and non-stationary time series analysis. *Proceedings of the Royal Society of London. Series A: mathematical, physical and engineering sciences, 454*(1971), 903-995.

Huang, R.-J., Zhang, Y., Bozzetti, C., Ho, K.-F., Cao, J.-J., Han, Y., et al. (2014). High secondary aerosol contribution to particulate pollution during haze events in China. *Nature, 514*(7521), 218-222.

Huang, R., Gu, L., Xu, Y.-h., Zhang, Q., Wu, S., & Cao, J. (2005). Characteristics of the interannual variations of onset and advance of the East Asian summer monsoon and their associations with thermal states of the tropical western Pacific. *Chinese J. Atmos. Sci, 29*(1), 20-36.

Jiang, X., Wang, Z., & Li, Z. (2018). Signature of the South China Sea summer monsoon onset on spring-to-summer transition of rainfall in the middle and lower reaches of the Yangtze River basin. *Climate Dynamics, 51*(9), 3785-3796.

Kajikawa, Y., & Wang, B. (2012). Interdecadal change of the South China Sea summer monsoon onset. *Journal of Climate, 25*(9), 3207-3218.

Kanamitsu, M., Ebisuzaki, W., Woollen, J., Yang, S.-K., Hnilo, J., Fiorino, M., & Potter, G. (2002). Ncep–doe amip-ii reanalysis (r-2). *Bulletin of the American Meteorological Society, 83*(11), 1631-1644.

Lelieveld, J., Evans, J. S., Fnais, M., Giannadaki, D., & Pozzer, A. (2015). The contribution of outdoor air pollution sources to premature mortality on a global scale. *Nature, 525*(7569), 367-371.

Li, K., Jacob, D. J., Liao, H., Qiu, Y., Shen, L., Zhai, S., et al. (2021). Ozone pollution in the North China Plain spreading into the late-winter haze season. *Proceedings of the national academy of sciences, 118*(10), e2015797118.

Li, K., Jacob, D. J., Liao, H., Shen, L., Zhang, Q., & Bates, K. H. (2019). Anthropogenic drivers of 2013–2017 trends in summer surface ozone in China. *Proceedings of the* national academy *of* sciences*, 116*(2), 422-427.

Li, K., Jacob, D. J., Shen, L., Lu, X., De Smedt, I., & Liao, H. (2020). Increases in surface ozone pollution in China from 2013 to 2019: anthropogenic and meteorological influences. *Atmospheric Chemistry and Physics, 20*(19), 11423-11433.

Lippmann, M. (1989). Health effects of ozone a critical review. *Japca, 39*(5), 672-695.

Liu, P., Song, H., Wang, T., Wang, F., Li, X., Miao, C., & Zhao, H. (2020). Effects of meteorological conditions and anthropogenic precursors on ground-level ozone concentrations in Chinese cities. *Environmental Pollution, 262*, 114366.

Lu, X., Hong, J., Zhang, L., Cooper, O. R., Schultz, M. G., Xu, X., et al. (2018).

Severe surface ozone pollution in China: a global perspective. *Environmental Science & Technology Letters, 5*(8), 487-494.

Lu, X., Zhang, L., Wang, X., Gao, M., Li, K., Zhang, Y., et al. (2020). Rapid increases in warm-season surface ozone and resulting health impact in China since 2013. *Environmental Science & Technology Letters, 7*(4), 240-247.

Sillman, S. (1995). The use of NO y, H2O2, and HNO3 as indicators for ozone-NO x-hydrocarbon sensitivity in urban locations. Journal of Geophysical Research: Atmospheres, 100(D7), 14175-14188.

Wan, R., & Wu, G. (2007). Mechanism of the spring persistent rains over southeastern China. *Science in China Series D: Earth Sciences, 50*(1), 130-144.

Wang, B., Huang, F., Wu, Z., Yang, J., Fu, X., & Kikuchi, K. (2009). Multi-scale climate variability of the South China Sea monsoon: A review. *Dynamics of Atmospheres and Oceans, 47*(1-3), 15-37.

Wang, B., Zhang, Y., & Lu, M. (2004). Definition of South China Sea monsoon onset and commencement of the East Asia summer monsoon. *Journal of Climate, 17*(4), 699-710.

Wang, L., & Chen, G. (2018). Relationship between South China Sea summer monsoon onset and landfalling tropical cyclone frequency in China. *International Journal of Climatology, 38*(7), 3209-3214.

Wang, N., Lyu, X., Deng, X., Huang, X., Jiang, F., & Ding, A. (2019). Aggravating O3 pollution due to NOx emission control in eastern China. *Science of the Total Environment, 677*, 732-744.

Wang, T., Xue, L., Brimblecombe, P., Lam, Y. F., Li, L., & Zhang, L. (2017). Ozone pollution in China: A review of concentrations, meteorological influences, chemical precursors, and effects. *Science of the Total Environment, 575*, 1582-1596.

Wang, Y., Gao, W., Wang, S., Song, T., Gong, Z., Ji, D., et al. (2020). Contrasting trends of PM2. 5 and surface-ozone concentrations in China from 2013 to 2017. *National Science Review, 7*(8), 1331-1339.

Wang, Z., Hu, B., Zhang, C., Atkinson, P. M., Wang, Z., Xu, K., et al. (2022). How the Air Clean Plan and carbon mitigation measures co-benefited China in PM2. 5 reduction and health from 2014 to 2020. *Environment International*, 169, 107510.

Xiang, B., & Wang, B. (2013). Mechanisms for the advanced Asian summer monsoon onset since the mid-to-late 1990s. *Journal of Climate, 26*(6), 1993-2009.

Xiao, X., Xu, Y., Zhang, X., Wang, F., Lu, X., Cai, Z., et al. (2022). Amplified Upward Trend of the Joint Occurrences of Heat and Ozone Extremes in China over 2013–20. *Bulletin of the American Meteorological Society, 103*(5), E1330-E1342.

Yang, Y., Li, M., Wang, H., Li, H., Wang, P., Li, K., et al. (2022). ENSO modulation of summertime tropospheric ozone over China. *Environmental Research Letters, 17*(3), 034020.

Yang, Y., Liao, H., & Li, J. (2014). Impacts of the East Asian summer monsoon on interannual variations of summertime surface-layer ozone concentrations over China. *Atmospheric Chemistry and Physics, 14*(13), 6867-6879.

Yin, Z., & Ma, X. (2020). Meteorological conditions contributed to changes in dominant patterns of summer ozone pollution in Eastern China. *Environmental*

Research Letters, 15(12), 124062.

Yin, Z., Wang, H., Li, Y., Ma, X., & Zhang, X. (2019). Links of climate variability in Arctic sea ice, Eurasian teleconnection pattern and summer surface ozone pollution in North China. *Atmospheric Chemistry and Physics, 19*(6), 3857-3871.

Yue, X., Unger, N., Harper, K., Xia, X., Liao, H., Zhu, T., et al. (2017). Ozone and haze pollution weakens net primary productivity in China. *Atmospheric Chemistry and Physics, 17*(9), 6073-6089.

Zhang, C., Jiang, Z., Liu, M., Dong, Y., & Li, J. (2023). Relationship between summer time near-surface ozone concentration and planetary boundary layer height in Beijing. Atmospheric Research, 106892.

Zhang, Q., Zheng, Y., Tong, D., Shao, M., Wang, S., Zhang, Y., et al. (2019a). Drivers of improved PM2. 5 air quality in China from 2013 to 2017. *Proceedings of the national academy of sciences, 116*(49), 24463-24469.

Zhang, X., Xiao, X., Wang, F., Brasseur, G., Chen, S., Wang, J., & Gao, M. (2022). Observed sensitivities of PM2. 5 and O3 extremes to meteorological conditions in China and implications for the future. *Environment International, 168*, 107428.

Zhang, Y., Zhou, W., & Leung, M. Y. (2019b). Phase relationship between summer and winter monsoons over the South China Sea: Indian Ocean and ENSO forcing. *Climate Dynamics, 52*(9), 5229-5248.

Zhao, Z., & Wang, Y. (2017). Influence of the West Pacific subtropical high on surface ozone daily variability in summertime over eastern China. *Atmospheric environment, 170*, 197-204.

Zhou, C., Wang, F., Guo, Y., Liu, C., Ji, D., Wang, Y., et al. (2023, March 24). Reconstructed daily ground-level MDA8 O_3 over 2005-2022 in China. [Dataset]. Zenodo. https://zenodo.org/record/7766129#.ZCGXAHZBw7F

Zhou, W., & Chan, J. C. (2005). Intraseasonal oscillations and the South China Sea summer monsoon onset. *International Journal of Climatology: A Journal of the Royal Meteorological Society, 25*(12), 1585-1609.

Zhou, W., & Chan, J. C. (2007). ENSO and the South China Sea summer monsoon onset. *International Journal of Climatology: A Journal of the Royal Meteorological Society, 27*(2), 157-167.

Zhou, W., Gao, M., He, Y., Wang, Q., Xie, C., Xu, W., et al. (2019). Response of aerosol chemistry to clean air action in Beijing, China: Insights from two-year ACSM measurements and model simulations. *Environmental Pollution, 255*, 113345.